UDC 004.621: 514 **doi: 10.32620/aktt.2026.3.10**

Qijie Li, S. Yepifanov

National Aerospace University "Kharkiv Aviation Institute", Ukraine
Anhui Jiebo Hypertron Avia. Tech Ltd., Co., China

CLOSED-FORM GEOMETRY AND ANALYTICAL PERFORMANCE ESTIMATES OF THE TWO-APEX WANKEL ROTARY COMPRESSOR

The **subject matter** of the article is the working-chamber geometry and the isentropic performance of the two-apex (m = 2) Wankel rotary compressor – a two-apex rotor orbiting within a single-lobe peritrochoid housing at a 2:1 eccentric-shaft gear ratio – a configuration geometrically well suited to gas compression yet, unlike the classical three-apex (m = 3) engine, it is almost unstudied analytically. The **goal** is to derive, rigorously and from first principles, the complete set of closed-form geometric and performance relations of the m=2 machine, exact expressions for which have not previously appeared in the literature, and to render the exact profiles manufac-turable. The **tasks** to be addressed are: to establish the kinematics and the 2:1 synchronizing-gear relation; to derive the exact housing and rotor (envelope) profiles together with the working-chamber area and volume laws; to obtain the displacement, compression ratio and apex-seal oscillation limit in closed form; to construct manufac-turable profiles that decouple the running clearance from the shape factor; and to develop the asymptotic scaling laws, the closed-form isentropic performance, and a design equation relating the ideal gain with any loss model. The **methods** used are: the differential geometry of trochoidal envelopes, Green's theorem for the chamber area and volume, the Taylor (asymptotic) expansion of the governing shape function, and closed-form isentropic thermo-dynamic analysis. The following **results** were obtained: the working-chamber volume law $V(t) = be^2[\Phi(K)/2 + 4Ksint]$, with $\Phi(K) = (K^2 + 8)arcsin(2/K) + 6\sqrt{(K^2 - 4)}$ and shape factor $K = R/e$, together with its exact crank-angle rate; exact theorems for the displacement $V_d = 8beR$ (about 54%larger than for $m = 3$ at identical e, R, b), the compression ratio $\varepsilon(K) = (\Phi + 8K)/(\Phi - 8K)$, and the apex-seal law $sin\varphi_{max} = 2/K$ giving $K_{min} = 4$ versus 6 for m = 3; exact normal parallel-offset profiles decoupling the running clearance S_p from K, removing the principal obstacle to precise CNC manufacture in earlier circular-arc treatments; four asymptotic design laws from a single expansion of $\Phi(K)$ — $\Phi - 8K = 16/(3K)$, $\varepsilon \approx 3K^2 + 1$ (within 1.3 % for $K \geq 4$), $V_{min}/V_d \approx 1/(3K^2)$(1 % clearance already at $K \approx 5.8$, no dead-volume machining), and $a \approx 2$: 1 volumetric-compactness advantage over m = 3 at the respective kinematic limits; and the isentropic indicated work in closed form, $W = p_0V_{max}/(\gamma - 1) \cdot \left[\varepsilon^{(\gamma-1)} - 1\right]$, yielding $IMEP \propto K^{0.80}$ and a strict monotonicity theorem. **Conclusions.** The scientific novelty of the results obtained is as follows: 1) for the first time the complete exact closed-form geometry of the $m = 2$ Wankel compressor was derived from first principles, rigorously quantifying its advantages over m = 3; 2) the exact normal parallel-offset method was developed, decoupling running clearance from shape factor and rendering the exact profile directly CNC-manufacturable, overcoming the chief limitation of earlier circular-arc practice; 3) the closed-form isentropic performance and the design equation $G(K^*) = L'(K^*)$ were obtained, separating the analytically known ideal gain from any loss model and providing a verified geometric and performance basis for subsequent thermodynamic and loss analysis.

Keywords: *Wankel rotary compressor; peritrochoid profile; shape factor; working process*; *thermodynamic analysis, design-space analysis*

1. Introduction

Wankel-type rotary-piston mechanisms originate in early rotary fluid devices [1] and were first realized in practice by Felix Wankel [2]; the dual-rotation DKM (Drehkolbenmotor, or dual-rotation rotary engine) was soon simplified by Froede and NSU Motorenwerke AG (commonly known as NSU) into the planetary KKM (*Kreiskolbenmotor*, or planetary rotary engine) – a stationary housing with an eccentrically orbiting rotor – that became the modern paradigm. Yamamoto [3] codified the principles of a viable rotary machine: purely rotary motion of every component, three-dimensionally reliable apex sealing, valveless port timing, structural integrity at high speed and pressure, and adequate cooling. These advantages drove major mid-century industrial investment and the classic monographs [4, 5]. Almost all of this development, however, concerns the three-apex ($m = 3$) engine.

Although the rotary engine's prospects remain contested – combustion instability and emissions in its elongated chamber – the same mechanism is increasingly attractive in non-combusting service as a compressor or expander [6, 7]. Here the very feature that handicaps the

engine becomes useful: the high chamber surface-to-volume ratio that causes wasteful heat loss in combustion instead aids heat rejection during compression. The valveless porting and the prospect of oil-free operation further suit high-purity duty – proton-exchange-membrane fuel cells [8], semiconductor, food and medical air [9] – where contamination is prohibited. Dry-sliding viability, long the chief obstacle, is being overcome by surface engineering such as diamond-like-carbon and micro-arc-oxidation coatings [10, 11], and a first industrial $m = 2$ compressor prototype [22] shows the configuration moving from laboratory curiosity toward engineered product.

The geometric theory of trochoidal machines is itself mature. Colbourne [13] established the differential geometry of epitrochoidal envelopes; Shung and Pennock [14] derived contact-force and volume relations for the general m -lobe family; the deviation-function method enabled integrated profile–seal co-design [15]; the rack method recently unified zero- and non-zero-clearance generation [16]; and parallel gerotor studies share the same epitrochoidal tooling [17]. Yet these treatments either target $m = 3$ or stay so general that closed-form design insight for a specific configuration is obscured, and apex-seal dynamics have likewise been analysed chiefly for $m = 3$ [18].

For the $m = 2$ compressor specifically, the pioneering systematic design procedure is due to Sukhomlinov [19], who, constrained by the computational tools of his era, approximated the exact epitrochoid by piecewise circular arcs and – more consequentially – conflated the shape factor with the running-clearance parameters. This coupling makes it impossible to prescribe the seal clearance independently of the shape factor, and therefore blocks high-precision numerically-controlled manufacture of the exact profile. Decoupling clearance from shape factor is thus a prerequisite for a manufacturable $m = 2$ compressor.

To the authors' knowledge, no published work gives exact closed-form expressions for the working-chamber volume law, theoretical displacement V_d, compression ratio $\varepsilon(K)$, or apex-seal oscillation limit $\phi_{\max}(K)$ of the $m = 2$ configuration: although Wankel [20] and Yamamoto [3] sketched $m = 2$ schematics and Colbourne's framework admits $m = 2$ as geometrically valid [13], none supplies these formulas, without which neither the $m = 2$ advantages over $m = 3$ nor the dependence of performance on the shape factor can be rigorously characterised. The present work closes this gap through a self-contained, exact mathematical analysis – no numerical model is used – with three linked contributions:

1. **Exact closed-form geometry.** From the exact envelope condition, we obtain the housing and rotor profiles, the working-chamber volume law $V(t) = be^2\left[\frac{\Phi(K)}{2} + 4K\sin t\right]$ together with its closed-form rate $\frac{\mathrm{d}V}{\mathrm{d}\alpha}$, the displacement $V_d = 8beR$, the compression ratio $\varepsilon(K) = \frac{\Phi+8K}{\Phi-8K}$, and the apex-seal law $\sin\phi_{\max} = \frac{2}{K}$ with $K_{\min} = 4$.
2. **Manufacturable profiles.** Exact normal-parallel-offset housing and rotor curves decouple the running clearance S_p from the shape factor K, rendering the exact profile directly CNC-ready and removing Sukhomlinov's principal limitation.
3. **Closed-form performance and design laws.** The isentropic indicated work $W = p_0 V_{\max}/\gamma - 1\,[\varepsilon^{\gamma-1} - 1]$ and IMEP; a Taylor expansion of $\Phi(K)$ giving $\varepsilon \approx 3K^2 + 1$, $\frac{V_{\min}}{V_d} \approx \frac{1}{3K^2}$ and IMEP $\sim K^{0.80}$; a strict monotonicity theorem; the $m = 2$–vs–$m = 3$ volumetric-compactness comparison; and the design equation $G(K^*) = L'(K^*)$ relating the analytically known ideal gain with any loss model.

The paper is organized as follows (here, the number indicates the section number): 1) sets up the kinematics and the 2: 1 synchronising gear; 2) derives the profiles and the area and volume laws by Green's theorem; 3) treats apex-seal kinematics and shape-factor admissibility; 4) gives the manufacturable normal-offset profiles; 5) compares $m = 2$ configuration with $m = 3$ classical configuration and quantifies volumetric compactness; 6) develops the asymptotic scaling laws; 7) derives the closed-form performance and the design equation; 8) concludes.

2. Geometric and Kinematic Framework

The $m = 2$ Wankel machine comprises three principal elements: an eccentric shaft, a two-apex rotor, and a single-lobe peritrochoid housing (see Fig. 1). Let α denote the eccentric-shaft (crank) angle. The rotor's self-rotation angle β about its own centre is locked to the shaft by

$$\beta = -\frac{\alpha}{2} \tag{1}$$

It is convenient to introduce the *working-chamber phase angle*

$$t \coloneqq -\beta = \frac{\alpha}{2}, \qquad t \in [0,2\pi), \tag{2}$$

so that one complete chamber cycle corresponds to t advancing through 2π (the shaft turning through 4π). The two fundamental design parameters are the eccentricity e (shaft-axis to rotor-centre offset) and the generating radius R (rotor circumradius); their ratio is the *shape factor*

ISSN 1814-4225 (print)
ISSN 2663-2012 (online)

$$K := \frac{R}{e}, \qquad K > 2, \tag{3}$$

with $K > 2$ the geometric admissibility condition (3.2). The axial width is b.

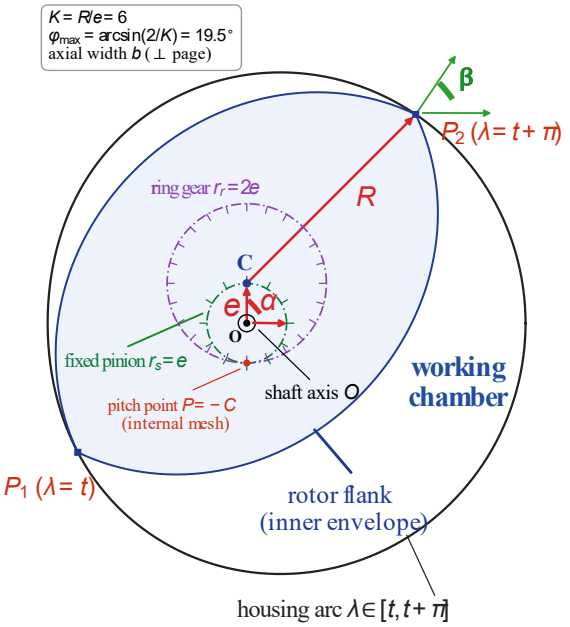

Fig. 1. Principal geometric parameters and working chamber mechanical assembly

Realization of the 2: 1 *timing*

The constraint (1) is enforced by an internal synchronizing gear pair: a stationary external pinion of pitch radius r_s, fixed to the side cover and coaxial with the shaft axis O, meshing internally with a ring gear of pitch radius r_r carried in the rotor bore and centred at the rotor centre C. With the ring rolling around the fixed pinion, the no-slip condition gives

$$\frac{\omega_{\text{rotor}}}{\omega_{\text{shaft}}} = 1 - \frac{Z_s}{Z_r} = 1 - \frac{r_s}{r_r}, \tag{4}$$

where Z_s, Z_r are the teeths numbers. Imposing $m = 2$, value $\frac{\omega_{\text{rotor}}}{\omega_{\text{shaft}}} = 1/2$, and $Z_r = 2Z_s$; hence,

$$r_s = e, \qquad r_r = 2e, \tag{5}$$

with internal-mesh center distance $r_r - r_s = e = |OC|$ and pitch point $P = -C$ (diametrically opposite the rotor center across O). The general m-machine requires $\frac{Z_r}{Z_s} = \frac{m+1}{m}$; the present result is its $m = 2$ specialisation. Since $r_r = 2e < R - 2e$ for all $K > 4$, the ring gear is contained within the rotor bore, confirming physical consistency.

3 Exact Profiles and the Working-Chamber Volume Law

3.1 Housing profile and the rotor flank as an exact envelope

Housing

The housing centerline is the base peritrochoid traced by an apex,

$$\boldsymbol{r}_0(\lambda) = (x_0, y_0) = \\ = (e\cos 2\lambda + R\cos\lambda,\ e\sin 2\lambda + R\sin\lambda), \\ \lambda \in [0, 2\pi), \tag{6}$$

with $|\boldsymbol{r}_0'| = \sqrt{R^2 + 4Re\cos\lambda + 4e^2}$ and outward unit normal $\boldsymbol{n}_h = (2e\cos 2\lambda + R\cos\lambda,\ 2e\sin 2\lambda + R\sin\lambda)/|\boldsymbol{r}_0'|$; the manufacturable wall is its parallel offset in Section 5.

Rotor frame

The rotor flank is the boundary the rotor body cannot cross – the *envelope*, seen from the rotor, of the housing family swept out as the shaft turns. Writing a planar point as the complex number $z = x + \mathrm{i}y$ and carrying a housing point into the rotor-fixed frame (translate by the rotor center $\boldsymbol{c}(t) = e\,\mathrm{e}^{\mathrm{i}2t}$, then rotate by $-t$ gives the one-parameter family

$$Z(\lambda, t) = \mathrm{e}^{-\mathrm{i}t}\left(e\,\mathrm{e}^{\mathrm{i}2\lambda} + R\,\mathrm{e}^{\mathrm{i}\lambda} - e\,\mathrm{e}^{\mathrm{i}2t}\right). \tag{7}$$

Envelope condition

A point lies on the envelope: if its λ- and t-derivatives are parallel, $\mathrm{Im}\left(\overline{Z_\lambda} Z_t\right) = 0$. Exact expansion gives $R\sin\lambda + R\sin(\lambda - 2t) + 2e\sin(2\lambda - 2t) = 0$, which the sum-to-product identities factor as

$$2\sin(\lambda - t)\ [R\cos t + 2e\cos(\lambda - t)\ ] = 0. \tag{8}$$

The first factor ($\lambda = t,\ t + \pi$) is the *apex-contact* branch—the two apex tips touching the housing at $\boldsymbol{r}_0(t)$ and $\boldsymbol{r}_0(t + \pi)$; the second is the *flank* branch.

Flank in closed form

Put $u := \lambda - t$; the flank branch reads $\cos t = -\left(\frac{2e}{R}\right)\cos u$, which has a real solution

$$R \geq 2e \quad \Leftrightarrow \quad K \geq 2, \tag{9}$$

recovering the admissibility condition (3). With $\Delta(u) := \sqrt{R^2 - 4e^2\cos^2 u}$ and $\sin t = \sigma\,\frac{\Delta(u)}{R}$ ($\sigma = \pm 1$, from $\sin^2 t + \cos^2 t = 1$), substituting $\lambda = t + u$ into (7) and simplifying exactly yields the base flank

$$X_0^{(\sigma)}(u) = \frac{\cos u}{R}\begin{pmatrix} R^2 + 4e^2\sin^2 u \\ -2\sigma e\,\Delta(u)\sin u \end{pmatrix}, \tag{10}$$

$$Y_0^{(\sigma)}(u) = \frac{\sin u}{R}\begin{pmatrix} R^2 - 4e^2\cos^2 u \\ -2\sigma e\,\Delta(u)\sin u \end{pmatrix}, \tag{11}$$

for $u \in [0, \pi]$, with apex tips $(X_0, Y_0)|_{u=0} = (R, 0)$ and $(X_0, Y_0)|_{u=\pi} = (-R, 0)$.

Branch selection

At the waist $u = \pi/2$, Eq. (11) gives $Y_0 = R - 2\sigma e$: the *inner* branch $\sigma = +1$ (waist $R - 2e$) is the physical flank, whereas $\sigma = -1$ (waist $R + 2e$) is the spurious outer envelope, which pierces the housing and must be discarded (Fig. 1). The complete two-apex rotor is the inner branch over $u \in [0, \pi]$ together with its mirror across the apex axis; its apexes contact the housing at phases t and $t + \pi$, matching the apex-contact branch.

3.2 Working chamber area and volume law

Because the axial width b is constant, the volume reduces to a planar problem,

$$V(\alpha) = b\, A_c(t), \qquad t = \alpha/2\,; \tag{12}$$

hence, it suffices to obtain the chamber cross-sectional area A_c. We do so directly by Green's theorem on the chamber boundary; the derivation is exact and its rate $\mathrm{d}V/\mathrm{d}\alpha$ is the source term of the future 0-D model.

Step 1 — chamber boundary

One working chamber is bounded by the fixed rotor flank and the housing arc swept between the two apex contacts, which by Section 2 occur at housing parameters $\lambda = t$ and $\lambda = t + \pi$ (see Fig. 2). With the housing point $\boldsymbol{r}_0(\lambda) = (x_0, y_0)$ of Eq. (6), Green's theorem gives

$$A_c(t) = A_{\text{flank}} + \frac{1}{2}\int_t^{t+\pi} (x_0\, \partial_\lambda y_0 - y_0\, \partial_\lambda x_0)\, \mathrm{d}\lambda\,, \tag{13}$$

where A_{flank} is the constant signed-area contribution of the flank.

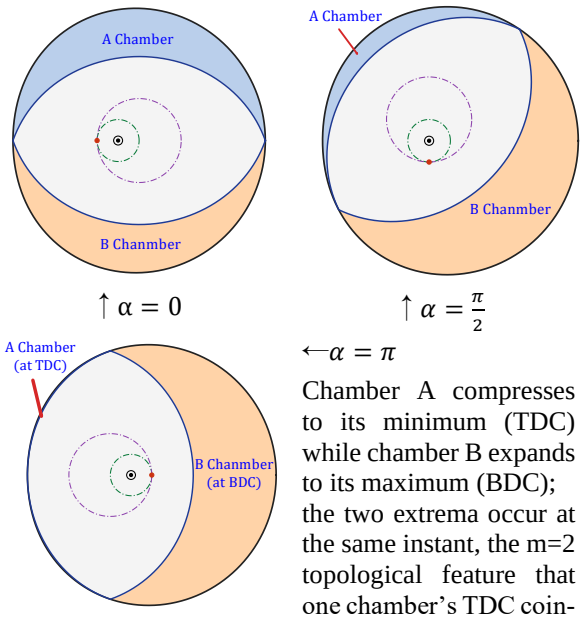

Chamber A compresses to its minimum (TDC) while chamber B expands to its maximum (BDC); the two extrema occur at the same instant, the m=2 topological feature that one chamber's TDC coincides with the other's BDC

Fig. 2. Working chamber evolution

Step 2 — the time-varying part

Substituting Eq. (6), the integrand evaluates in closed form to

$$\begin{gathered} x_0\, \partial_\lambda y_0 - y_0\, \partial_\lambda x_0 = \\ = -R^2 - 3Re\cos\lambda + Re\cos(\lambda - 2t) + \\ + 2e^2 \cos(2\lambda - 2t) - 2e^2. \end{gathered} \tag{14}$$

Over the half-period only the two single-angle cosines survive: $\int_t^{t+\pi} \cos\lambda\, \mathrm{d}\lambda = -2\sin t$ and $\int_t^{t+\pi} \cos(\lambda - 2t)\, \mathrm{d}\lambda = +2\sin t$, while $\cos(2\lambda - 2t)$ integrates to zero, giving

$$\begin{gathered} \int_t^{t+\pi} (x_0\, dy_0 - y_0\, dx_0) = \\ = -\pi(R^2 + 2e^2) + 8Re\sin t, \end{gathered} \tag{15}$$

so that $A_c(t) = C + 4Re\sin t$: the chamber area is an exact sinusoid in $t = \alpha/2$.

Step 3. The constant, and the role of ϕ_{max}

Mirror symmetry at $t = 0$ makes the two chambers equal, fixing $C = A_f/2$ with $A_f = A_h - A_r$ the total free area. Green's theorem on the closed housing and rotor curves gives, in exact closed form,

$$A_h = \frac{1}{2}\oint (x_0\, dy_0 - y_0\, dx_0) = \pi(R^2 + 2e^2), \tag{16}$$

$$\begin{gathered} A_r = \pi(R^2 + 2e^2) - \\ - \left[(R^2 + 8e^2)\arcsin\frac{2e}{R} + 6e\sqrt{R^2 - 4e^2}\right], \end{gathered} \tag{17}$$

the arcsin arising from the exact integration of the flank radical $\sqrt{R^2 - 4e^2\cos^2 u}$. Hence,

$$\begin{gathered} A_c(t) = \frac{A_f}{2} + 4Re\sin t, \\ A_f = (R^2 + 8e^2)\arcsin 2e/R + 6e\sqrt{R^2 - 4e^2}. \end{gathered} \tag{18}$$

Remark 3.1 The constant $\arcsin(2e/R)$ in Eq. (18) is precisely the apex-seal swing limit $\phi\_\max = \arcsin(2/K)$ of ***Proposition 4.1***: the angle that bounds the seal kinematics re-enters as the central constant of the area law, $A_f = (R^2 + 8e^2)\,\phi_{\max} + 6e\sqrt{R^2 - 4e^2}$. The static interference angle is thus also the governing constant of the chamber thermodynamics.

Step 4. Volume law and its rate

With $R = Ke$ and

$$\begin{gathered} \Phi(K) = (\mathrm{K}^2 + 8)\arcsin\frac{2}{K} + 6\sqrt{K^2 - 4}, \\ K > 2, \end{gathered} \tag{19}$$

ISSN 1814-4225 (print)
ISSN 2663-2012 (online)

one has $A_f = e^2\Phi(K)$; multiplying Eq. (18) by b yields the volume law.

Theorem 3.1 *The working-chamber evolution is shown in Fig. 2. Volume and its crank-angle derivative are*

$$V(\alpha) = be^2\left[\frac{\Phi(K)}{2} + 4K\sin\frac{\alpha}{2}\right] = \\ = V_{\min} + 4bRe\left(1+\sin\frac{\alpha}{2}\right), \qquad (20)$$

$$\frac{\mathrm{d}V}{\mathrm{d}\alpha} = 2bRe\cos\left(\frac{\alpha}{2}\right), \qquad (21)$$

3.3 Displacement and compression ratio

Proposition 3.2
$V_{\max} = be^2\left[\frac{\Phi}{2} + 4K\right]$ *at* $t = \frac{\pi}{2}$ *and*
$V_{\min} = be^2\left[\frac{\Phi}{2} - 4K\right]$ *at* $t = \frac{3\pi}{2}$;
$V_{\min} > 0 \Leftrightarrow \Phi(K) > 8K$, *which holds for all* $K > 2$.

Theorem 3.3 Displacement and compression ratio.

$$V_d = V_{\max} - V_{\min} = 8be^2K = 8beR, \\ \varepsilon(K) = \frac{V_{max}}{V_{min}} = \frac{\Phi(K) + 8K}{\Phi(K) - 8K}. \qquad (22)$$

Remark 3.2 From ***Proposition 3.2,*** we obtain $V_{\min} = be^2/2\,(\Phi - 8K)$, i.e. the denominator $\Phi - 8K$ of ε is exactly proportional to the minimum chamber volume (coefficient $\frac{be^2}{2}$). This identity underlies the asymptotic laws of Section 7.

4 Apex-Seal Kinematics and Shape-Factor Admissibility

Each rotor apex carries a radial seal sliding in a rotor slot; as the rotor orbits, the seal tilts to follow the housing. The maximum tilt sets the tribological severity and a lower bound on K.

Proposition 4.1 Apex-seal maximum oscillation.

$$\mathrm{Sin}\phi_{\max} = \frac{2e}{R} = \frac{2}{K}. \qquad (23)$$

The general m-machine obeys $\sin\phi_{\max} = m/K$, *consistent with the $m = 3$ result $3/K$ of [3].*

Asymmetric shape-factor bounds for a compressor.

The two ends of the admissible K range are bounded by physically different mechanisms, and the distinction is sharper for a compressor than for the engine the 30° rule was devised for. The *lower* bound is a hard kinematic red line: it follows purely from apex-seal geometry Eq. (23) and binds any trochoidal machine – engine or compressor – because excessive seal tilt causes leakage and wear regardless of the working process. The conventional *upper* bound $K \le 8$ quoted for engines, by contrast, is a *combustion* constraint: large K drives ε_{th} toward knock, and the long, flat chamber has a high surface-to-volume ratio that quenches the flame. Neither applies to a non-combusting compressor – indeed a high surface-to-volume ratio is here *beneficial*, enhancing heat rejection so the process tends toward the work-minimizing isothermal limit. The practical ceiling on K for a compressor is therefore not thermodynamic but three-dimensional and mechanical: large K means small eccentricity relative to R, so that **(i)** the displacement per unit installed volume falls—the volumetric-compactness penalty quantified in Section 6; **(ii)** the top-dead-center clearance becomes very thin, constraining valve placement and tolerancing; and **(iii)** the eccentric-shaft journals nearly coincide, limiting bearing strength.

An $m = 2$ compressor is thus free to exploit shape factors well above the engine convention, bounded by packaging rather than by combustion.

5 Manufacturable Profiles via Normal Parallel Offset

The base curves Eq. (6) – Eq. (11) define a zero-clearance pair. A physical machine requires a controlled running clearance, introduced as an *exact normal parallel offset* of each base curve along its own outward unit normal (see Fig. 3):

$$\text{housing wall:} \quad \boldsymbol{R}_h(t) = \boldsymbol{r}_0(t) + a\,\boldsymbol{n}_h(t), \qquad (25)$$
$$\text{rotor flank:} \quad \boldsymbol{R}_{\mathrm{rot}}(u) = \boldsymbol{r}_{\mathrm{flank}}(u) + a'\,\boldsymbol{n}_{\mathrm{rot}}(u), \qquad (26)$$
$$a' = a - S_p,$$

where a is the housing offset, a' the rotor offset, and $S_p = a - a'$ is the resulting apex/flank running clearance.

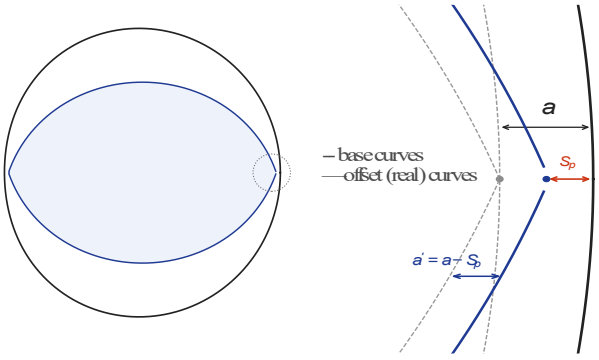

(a) Full machine with the offset (real) housing wall and rotor.

(b) Apex detail: base curves (dashed) and their normal offsets (solid);

Offsets are exaggerated for legibility.

Fig. 3. Profiles via normal parallel offset

Proposition 5.1 Clearance–shape-factor decoupling.

The running clearance $S_p = a - a'$ in Eq. (26) is an independent design parameter: it may be prescribed to any value without changing the shape factor K. The displacement $V_d = 8beR$ and compression ratio $\varepsilon(K)$ of ***Theorem 3.3*** *are the nominal (zero-clearance, base-curve) values; the offset perturbs the realized volumes only at first order in a/e, a'/e.*

Remark 5.1 The offset adds a thin dead-volume layer that raises the minimum chamber volume to $V_{\min}^{\text{eff}} = V_{\min} + \Delta V_c(S_p)$, lowering the effective ratio to $\varepsilon_{\text{eff}} = V_{\max}^{\text{eff}}/V_{\min}^{\text{eff}} \le \varepsilon(K)$. Because $V_{\min}$ is small as in ***Proposition 7.3***, ε is comparatively sensitive to clearance; the correction ΔV_c follows directly from the offset profiles Eq. (25) – Eq. (26) and should be carried whenever high precision in ε is required. The decoupling makes this an independently tunable correction rather than one entangled with K.

This decoupling is the key enabler for precise manufacture. Earlier design practice approximated the trochoid by circular arcs and, in doing so, conflated the shape factor with the clearance, so that the running gap could not be specified independently of K. Equations (25) – (26) remove this coupling: the exact profiles, offset by a prescribed S_p along the analytic normal, are directly suitable for numerically-controlled CNC machining to sub-micron fidelity.

6 Design Space: Comparison with m = 3 and Volumetric Compactness

6.1 Comparison with the classical m = 3 machine

Table.1 collects the closed-form results against the $m = 3$ Wankel.

Table 1.
Closed-form comparison of m=2 and m=3 machines (same e,R,b).

Property	$m = 2$	$m = 3$
Kinematic constraint	$\beta = -\alpha/2$	$\beta = -\alpha/3$
Gear ratio $Z_r : Z_s$	2: 1	3: 2
Displacement V_d	$8eRb$	$3\sqrt{3}\,eRb \approx 5.196\,eRb$
Ratio $V_d^{(2)}/V_d^{(3)}$	$8/(3\sqrt{3}) \approx 1.540$	
$\sin\phi_{max}$	$2/K$	$3/K$
K_{min} ($\phi_{max} \le 30°$)	4	6
Admissibility	$K > 2$	$K > 3$

For identical e, R, b, the $m = 2$ machine delivers about 54% more swept volume, while its lower apex-seal demand and lower $K_{\min}$ widen the admissible design space.

6.2 Volumetric compactness

For a machine of fixed external sizeб the natural figure of merit is the displacement delivered per unit enclosed volume. The rotor apex reaches a maximum distance $R_{\text{env}} = R + e = e(K+1)$ from the shaft axis, so the smallest cylinder enclosing the machine has volume $V_{\text{env}} = \pi R_{\text{env}}^2 b$, We define the *volumetric compactness*

$$\eta_{\text{env}}(K) = \frac{V_d}{V_{\text{env}}} = \frac{8}{\pi}\frac{K}{(K+1)^2},$$
$$\frac{\mathrm{d}\eta_{\text{env}}}{\mathrm{d}K} = \frac{8}{\pi}\frac{1-K}{(K+1)^3} < 0 \quad (K > 1). \qquad (27)$$

The bounding cylinder being a common yardstick that applies equally to both configurations.

Compactness therefore decreases monotonically over the admissible range (see Fig. 4). Comparing each configuration at its own kinematic limit,

$$\frac{\eta_{\text{env}}^{(m=2)}(4)}{\eta_{\text{env}}^{(m=3)}(6)} = \frac{32/25}{18\sqrt{3}/49} \approx 2.01, \qquad (28)$$

i.e. at its $K_{\min} = 4$, the $m = 2$ machine is roughly twice as volumetrically dense as the $m = 3$ machine at its $K_{\min} = 6$.

η_{env} is a first-order proxy for material cost in volume production: more displacement per enclosed volume means less housing and rotor, and a smaller, lighter machine per unit output. It is therefore an economically meaningful figure of merit fixed entirely by the geometry.

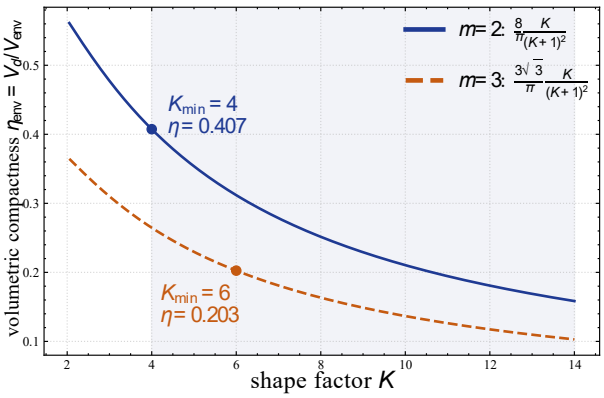

Fig. 4. Volumetric compactness $\eta_{\text{env}}(K) = V_d/V_{\text{env}}$ for m = 2 and m = 3

7 Asymptotic Scaling Laws

A single Taylor expansion of $\Phi(K)$ generates the engineering scaling laws.

ISSN 1814-4225 (print)
ISSN 2663-2012 (online)

Proposition 7.1 (Clearance asymptotic).

$$\Phi(K) - 8K = \frac{16}{3K} + O(K^{-3}) \qquad (K \to \infty). \qquad (29)$$

Proof. With $\arcsin(2/K) = 2/K + 4/(3K^3) + O(K^{-5})$ and $\sqrt{K^2-4} = K - 2/K + O(K^{-3})$,

$$\Phi(K) = \underset{\to\infty}{2K} + \frac{52}{3K} + \underset{\to\infty}{6K} - \frac{36}{3K} + O(K^{-3})$$
$$= 8K + \frac{16}{3K} + O(K^{-3}).$$

The two individually divergent leading parts $2K$ and $6K$ sum to exactly $8K$ and cancel against $-8K$; the finite remainder is $16/(3K)$.

Corollary 7.2 (Quadratic compression-ratio law).

$$\varepsilon(K) = 1 + \frac{16K}{\Phi - 8K} = 3K^2 + 1 + O(K^{-2}), \qquad (30)$$

the identity in the first equality being exact; the relative error of $\varepsilon \approx 3K^2 + 1$ is below 1.3% for all $K \geq 4$ (e.g. $K = 4$: 48.4 vs 49; $K = 6$: 108.4 vs 109).

The diagrams for the compression ratio and its error are shown in Fig. 5, a, b.

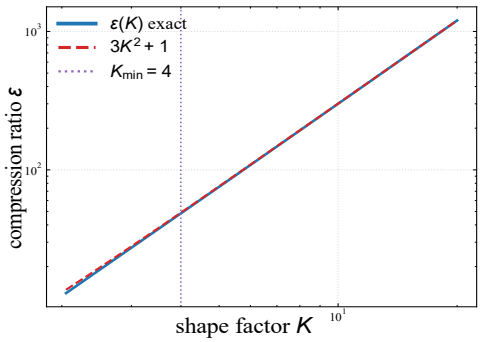

(a)

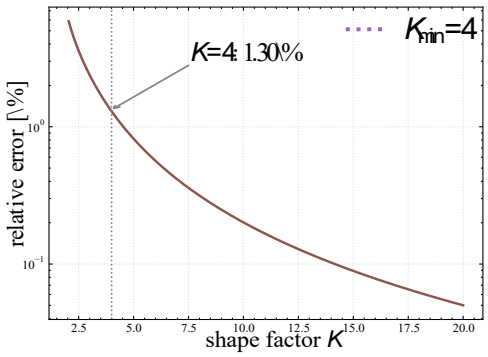

(b)

Fig. 5. Quadratic compression-ratio law:
a – ε(K) and the asymptotic $3K^2 + 1$ on log–log axes;
b – relative error, below 1.3% for all $K \geq K_{min} = 4$

Proposition 7.3 (Self-regulating clearance ratio).

$$\frac{V_{min}}{V_d} = \frac{1}{3K^2} + O(K^{-4}); \qquad (31)$$

hence, a 1% clearance ratio is reached at $K \approx 5.8$, within the admissible range, with no dead-volume machining.

The maximum and minimum volumes vs *K* are presented in Fig. 6, a; the clearance ratio is presented in Fig. 6, b.

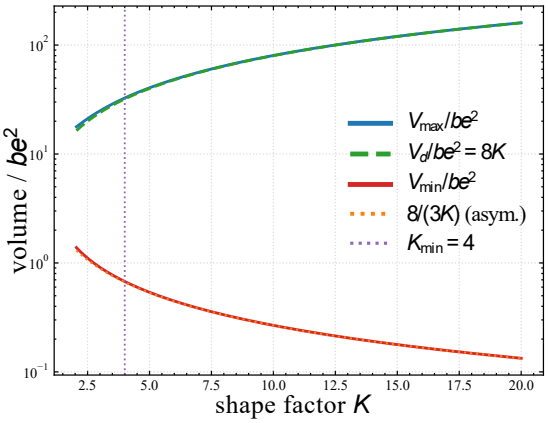

(a)

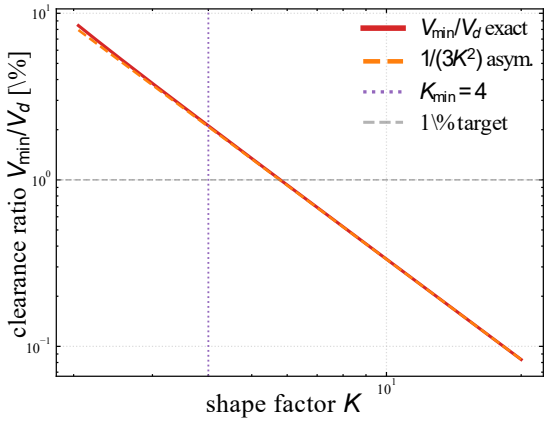

(b)

Fig. 6. Clearance volume:
a – $V_{max}, V_d = 8K, V_{min}$ (normalised by be^2) with the $8/(3K)$; b – the clearance ratio $V_{min}/V_d \approx 1/(3K^2)$ (slope -2), reaching the 1% target at $K \approx 5.8$

8 Closed-Form Isentropic Performance and the Design Equation

Treating the compression as a reversible adiabatic (isentropic) process, $pV^\gamma = \text{const}$, the indicated work follows in *closed form* directly from the analytic volume law—no numerical integration is required.

Theorem 8.1 (Closed-form isentropic indicated work).

For isentropic compression from V_{max} (pressure p_0) to V_{min},

$$W = \frac{p_0 V_{max}}{\gamma - 1}[\varepsilon^{\gamma-1} - 1],$$
$$\frac{\text{IMEP}}{p_0} = \frac{W}{p_0 V_d} = \frac{1}{\gamma - 1}\frac{\varepsilon}{\varepsilon - 1}(\varepsilon^{\gamma-1} - 1). \qquad (32)$$

Proposition 8.2 (IMEP power law).

As $K \to \infty$, $\frac{\mathrm{IMEP}}{p_0} \sim \frac{3^{\gamma-1}}{\gamma-1} K^{2(\gamma-1)}$; *for air* ($\gamma \approx 1.40$), *the exponent approximately is* 0.80, *a strictly sub-linear, diminishing-returns law.*

Theorem 8.3 (Strict monotonicity).

Under the isentropic model $\mathrm{IMEP}(K)$ *is strictly increasing for all* $K > 2$, *with* $\mathrm{d}(\mathrm{IMEP}/p_0)/\mathrm{d}K \geq 1.70$ *on* $K \in [2.01, 20]$ *(numerically confirmed lower bound; analytically,* $\varepsilon'(K) > 0$ *and* $f(\varepsilon) = \varepsilon/\varepsilon - 1\,(\varepsilon^{\gamma-1} - 1)$ *is increasing).*

Corollary 8.4 (No finite interior optimum; the design equation).

The unconstrained problem $\max_{K>2}\mathrm{IMEP}(K)$ *is unbounded: the optimum is set by constraints/losses, not by a thermodynamic extremum. See Fig. 7.*

Writing the marginal gain $G(K) := \mathrm{d}(\mathrm{IMEP}/p_0)/\mathrm{d}K \sim K^{-0.20}$ *and any loss term* $L(K)$ *increasing in* K, *the net metric* $\Pi(K) = \mathrm{IMEP} - p_0 L(K)$ *attains its interior maximum at*

$$G(K^*) = L'(K^*). \qquad (33)$$

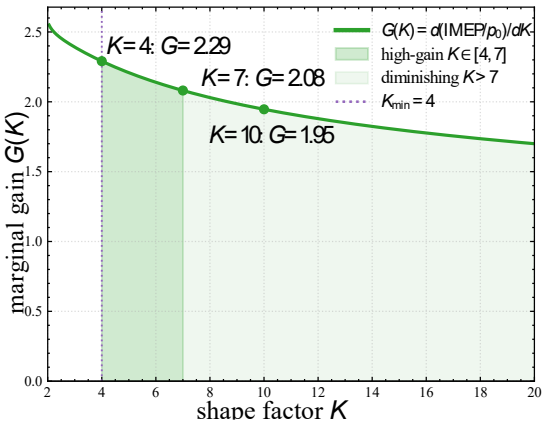

Fig. 7. Marginal gain $\mathrm{G(K)} = \mathrm{d(IMEP/p_0)/dK}$

Remark 8.1 $G(K)$ is the *marginal thermodynamic gain* (the derivative of the relative IMEP), *not* a loss. Eq.(33) separates roles cleanly: $G(K^*)$ is known analytically from the ideal model, while $L'(K^*)$ is the only quantity a loss model must supply. In this paper, $L(K)$ is left symbolic (e.g. $L' = aK$); a quantitative loss model is outside the present (loss-free, analytic) scope.

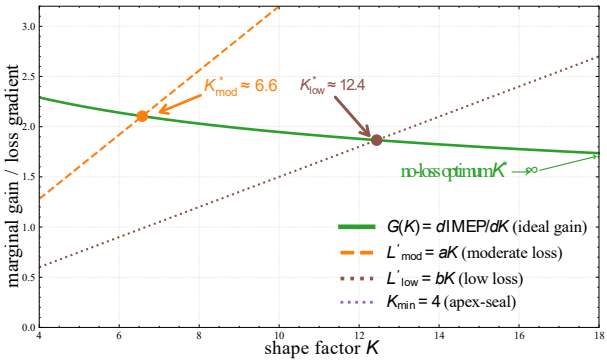

Fig. 8. Solutions of the design equation $\mathrm{G}(K^*) = \mathrm{L}'(K^*)$

As Fig. 8 shows, the ideal gain $G(K)$ crossed by two illustrative loss gradients $L' = aK$, locating $K^* \approx 6.6$ (moderate loss) and $K^* \approx 12.4$ (low loss); as losses vanish, $K^* \to \infty$.

Conclusions

For the $m = 2$ Wankel rotary compressor, we have derived in exact closed form: the synchronising 2: 1 gear relation; the housing and rotor profiles; the working-chamber area and volume laws via $\Phi(K)$; the displacement $V_d = 8beR$, compression ratio $\varepsilon(K)$, and apex-seal law $\sin\phi_{\max} = 2/K$ with $K_{\min} = 4$; the manufacturable normal-offset profiles that decouple running clearance from shape factor; a volumetric- compactness comparison giving a 2: 1 density advantage over $m = 3$ at the respective kinematic limits; the asymptotic laws $\Phi - 8K = 16/(3K)$, $\varepsilon = 3K^2 + 1$, $V_{\min}/V_d = 1/(3K^2)$; and the closed-form isentropic work, $\mathrm{IMEP} \sim K^{0.80}$, with a strict monotonicity theorem and the design equation $G(K^*) = L'(K^*)$.

All results are exact or asymptotic; no numerical model is invoked. The further paper shall develop a zero-dimensional numerical isentropic model that takes the present closed forms as its geometric input and is cross-checked against the closed-form work of ***Theorem 8.1***; the loss term $L(K)$ required to close Eq. (33), together with heat transfer and valve dynamics, is deferred to subsequent work.

Contributions of authors: conceptualization, methodology – **Li Qijie, S. Yepifanov;** formulation of tasks, analysis **– Li Qijie, S. Yepifanov;** development of model – **Li Qijie;** analysis of results, visualization **– Li Qijie;** writing – **Li Qijie;** original draft preparation – **S. Yepifanov**, writing – review and editing **– Li Qijie, S. Yepifanov.**

Conflict of Interest

The authors declare that they have no conflict of interest in relation to this research, whether financial,

personal, authorship or otherwise, that could affect the research and its results presented in this paper.

Financing

This study was conducted without financial support.

Data Availability

The work has associated data that can be provided upon reasonable request.

Use of Artificial Intelligence

The authors confirm that they did not use artificial intelligence methods while creating the presented work.

All the authors have read and agreed to the published version of this manuscript.

References

1. Ramelli, A. *Le Diverse et Artificiose Machine del Capitano Agostino Ramelli*. Paris : Casa dell'Autore, 1588. 722 p.

2. Wankel, F. *Drehkolbenbrennkraftmaschine*. Patent DE, № 943542, 1954.

3. Yamamoto, K. *Rotary Engine.* Tokyo, Sankaido, 1981. 67 p.

4. Ansdale, R. F., Lockley, D. J. *The Wankel RC Engine: Design and Performance*. South Brunswick, A. S. Barnes, 1969. 166 p.

5. Norbye, J. P. *The Wankel Engine: Design, Development, Applications*. Philadelphia, Chilton Book Co., 1971. 518 p.

6. Imran, M., Usman, M., Park, B. S., Lee, D. H. Volumetric Expanders for Low Grade Heat and Waste Heat Recovery Applications. *Renewable and Sustainable Energy Reviews*, 2016, vol. 57, pp. 1090-1109.

7. Taskin, A., Farrukh, S., LomiGa, J., Mahmoud, S., Al-Dadah, R. Innovative Design and Performance Analysis of a Static Shaft Wankel Expander for Micro-Scale Organic Rankine Cycles. *Energy Conversion and Management*, 2025, vol. 325. 15 p.

8. Liang, X., Kang, H., Shen, J., Li, Z., Zeng, R. Review and Analysis of Hydrogen Recirculation Devices for Compact Vehicular Proton Exchange Membrane Fuel Cells. Journal of Power Sources, 2023, vol. 555. 20 p.

9. Marshall, R. Meeting ISO 8573-1 compressed air quality specifications. *Air Best Practices*. Approx, 2025. 8 p.

10. Nakatani, T., Okamoto, K., Araki, A., Washimi, T. Application of Diamond-like Carbon to a Rotary Engine. *New Diamond and Frontier Carbon Technology*, 2006, vol. 16, iss. 4, pp. 187-196.

11. Gupta, A., Jayaram, S., McCormick, H. E. Identification of Materials and Coatings to Minimise/Eliminate Wankel Rotary Engine's Apex Seal/Trochoid Wear Chatter. *International Journal of Surface Science and Engineering*, 2020, vol. 14, iss. 2, pp. 135-157.

12. Yu, X., Zhao, D. A Foreign-Academician Workstation in Our City Exhibits Its Products at the World Manufacturing Convention. Huaibei Daily, 2022. 2 p. (in Chinese).

13. Colbourne, J. R. The Geometry of Trochoid Envelopes and Their Application in Rotary Pumps. *Mechanism and Machine Theory*, 1974, vol. 9, iss. 3, pp. 421-435.

14. Shung, J. B., Pennock, G. R. Geometry for Trochoidal-Type Machines with Conjugate Envelopes. *Mechanism and Machine Theory*, 1994, vol. 29, iss. 1, pp. 25-42.

15. Warren Rose, S., Yang, D. C. H. The Deviation Function Method of Rotary Engine Design by Geometric Parameters. *Journal of Mechanical Design*, 2014, vol. 136, iss. 5. 7 p.

16. Lacevic, H., Kovacevic, A., Stosic, N., Read, M. Application of Rack Method in Generation of Internally Geared Rotor Profiles. *Mechanism and Machine Theory*, 2025, vol. 215. 18 p.

17. Robison, A. J., Vacca, A. Performance Comparison of Epitrochoidal, Hypotrochoidal, and Cycloidal Gerotor Gear Profiles. *Mechanism and Machine Theory*, 2021, vol. 158. 26 p.

18. Pennock, G. R., Beard, J. E. Force Analysis of the Apex Seals in the Wankel Rotary Compressor Including the Influence of Fluctuations in the Crankshaft Speed. *Mechanism and Machine Theory*, 1997, vol. 32, iss. 3, pp. 349-361.

19. Sukhomlynov, R. M. *Trokhoydnye rotornye kompressory* [Trochoid rotor compressors]. Kharkiv, Vyshcha shkola, 1975. 152 p.

20. Wankel, F. Rotary Piston Machines: Classification of Design Principles for Engines, Pumps and Compressors. London : Iliffe Books, 1965. 64 p.

Received 02.06.2026, Received in revised form 14.06.2026
Accepted date 15.06.2026, Published date 17.06.2026

ГЕОМЕТРИЧНІ РОЗРАХУНКИ ТА АНАЛІТИЧНІ ОЦІНКИ ХАРАКТЕРИСТИК ДВОВЕРШИННОГО РОТОРНОГО КОМПРЕСОРА ВАНКЕЛЯ

Лі Цицзе, С. В. Єпіфанов

Предметом статті є геометрія робочої камери та ізоентропічні характеристики двовершинного (m = 2) роторного компресора Ванкеля — двовершинного ротора, що обертається в однопелюстковому перитрохоїдному корпусі з ексцентриковим передаточним числом 2:1. Ця геометрична конфігурація,

добре пристосована для стиснення газу, але, на відміну від класичного тривершинного (m = 3) варіанта, майже не вивчена аналітично. **Мета** полягає в тому, щоб для конфігурації m=2 отримати повний набір геометричних і робочих співвідношень замкнутої форми, точні вирази для яких раніше не з'являлися в літературі, та зробити точні профілі придатними для виробництва. **Завдання**, які необхідно вирішити: встановити кінематику та співвідношення синхронізуючої передачі 2:1; вивести точні профілі корпусу та ротора (оболонки) разом із законами площі та об'єму робочої камери; отримати переміщення, ступінь стиснення та межу коливань вершинного ущільнення в замкнутій формі; побудувати придатні для виробництва профілі, що відокремлюють робочий зазор від коефіцієнта форми; а також розробити асимптотичні закони масштабування, рівняння для визначення ізоентропійних характеристик та рівняння проєктування, що зв'язує ідеальний коефіцієнт підсилення з моделлю втрат. Використані **методи**: диференціальна геометрія трохоїдальних обвідних, теорема Гріна для площі та об'єму камери, розкладання Тейлора (асимптотичне) для визначальної функції форми та ізоентропійний термодинамічний аналіз замкнутої форми. Отримано такі **результати**: закон зміни об'єму робочої камери за кутовим положенням колінчастого вала $V(t) = be^2[\Phi(K)/2 + 4Ksint]$, де $\Phi(K) = (K^2 + 8)arcsin(2/K) + 6\sqrt{(K^2 - 4)}$, $K = \frac{R}{e}$ - коефіцієнт форми; точна формула для переміщення $V_d = 8beR$ (для m=2 це значення на 54% вище ніж для $m = 3$ при тих самих e, R, b), ступінь стиснення $\varepsilon(K) = (\Phi + 8K)/(\Phi - 8K)$, закон зміни апекс-ущільнення $sin\varphi_{max} = \frac{2}{K}$, що дає $K_{min} = 4$ замість 6 для m = 3; точні нормальні профілі паралельного зміщення, що визначають залежність радіального зазору S_p від K, усуваючи головну перешкоду для точного ЧПК-виробництва, яке раніше було основане на заміні реальної лінії коловими дугами; асимптотичні закони проєктування, отримані як наслідок асимптотичної заміни $\Phi - 8K \approx 16/(3K)$: $\varepsilon \approx 3K^2 + 1$, $V_{min}/V_d \approx 1/(3K^2)$, $a \approx 2{:}1$; формула для ізоентропної роботи $W = p_0V_{max}/(\gamma - 1) \cdot \left[\varepsilon^{(\gamma-1)} - 1\right]$, з якої випливає $IMEP \propto K^{0.80}$, а також теорема про сувору монотонність. **Наукова новизна** отриманих результатів полягає в наступному: 1) вперше отримано в замкнутій формі систему рівнянь, які визначають повну точну геометрію компресора Ванкеля для m=2, що дозволило кількісно визначити його переваги над схемою з m = 3; 2) розроблено точний нормальний метод паралельного зміщення, який визначає залежність робочого зазору від коефіцієнта форми та вможливлює виготовлення точного профілю безпосередньо на верстатах з ЧПК, долаючи головне обмеження попередньої практики, основаної на апроксимації профілю круговими дугами; 3) отримано рівняння проєктування $G(K^*) = L'(K^*)$, які визначають зв'язок аналітичного виразу для підсилення із заданою в будь-якій формі моделлю втрат та створюють перевірену геометричну та експлуатаційну основу для подальшого термодинамічного аналізу робочого процесу компресора зазначеного типу.

Ключові слова: роторний компресор Ванкеля; перітрохоідний профіль; форм-фактор; робочий процес; термодинамічний аналіз; проєктуваня

Цицзе Лі – аспірант каф. конструкції авіаційних двигунів, Національний аерокосмічний університет «Харківський авіаційний інститут», Харків, Україна; компанія Anhui Jiebo Hypertron Avia. Tech Ltd., Co., China.

Єпіфанов Сергій Валерійович – д-р. техн. наук., проф., зав. каф. конструкції авіаційних двигунів, Національний аерокосмічний університет «Харківській авіаційний інститут», Харків, Україна.

Qijie Li – post-graduate student at the Department of Aircraft Engines Design, National Aerospace University "Kharkiv aviation Institute", Kharkiv, Ukraine,
e-mail: qijie_hit@yahoo.com, ORCID: 0000-0002-7295-6373.

Sergiy Yepifanov – Dr. of Sc. in Engineering, Prof., Head of Engine Design Department, National Aerospace University «Kharkiv Aviation Institute», Kharkiv, Ukraine,
e-mail: s.yepifanov@khai.edu, ORCID: 0000-0003-0533-9524, Scopus ID: 6506749318.